ELSEVIER

Journal of Fluids and Structures 24 (2008) 481–495

JOURNAL OF FLUIDS AND STRUCTURES

www.elsevier.com/locate/jfs

Free-stream turbulence effects on vortex-induced vibration and flow-induced force of an elastic cylinder

R.M.C. So[a,*], X.Q. Wang[a], W.-C. Xie[b], J. Zhu[b]

[a]*Department of Mechanical Engineering, The Hong Kong Polytechnic University, Hung Hom, Kowloon, Hong Kong SAR, China*
[b]*Department of Civil and Environmental Engineering, Faculty of Engineering, University of Waterloo, Waterloo, Ont., Canada*

Received 15 February 2007; accepted 22 October 2007
Available online 21 February 2008

Abstract

The effect of free-stream turbulence on vortex-induced vibration of an elastic cylinder in a cross-flow and the associated fluid forces was investigated experimentally. The range of Reynolds number investigated is 5000–41 000. A turbulence generation grid was used to generate turbulence intensity around 10% in the upstream flow. Cylinder displacements in the transverse direction at cylinder mid-span were measured in the reduced velocity range $U_{r0} = 1.45$–12.08. The cylinder vibration has two dominant components, one at the frequency of vortex shedding and another at the natural frequency of the fluid-cylinder system. These are represented by their root-mean-square (r.m.s) values, w'_{yV} and w'_{yM}, respectively. For a nonturbulent uniform flow, w'_{yV} is dominant in the U_{r0} range of $1.45 < U_{r0} < 7.25$, where lock-in occurs at $U_{r0} = 5.31$, while w'_{yM} is dominant in the post-lock-in U_{r0} range of $8.21 < U_{r0} < 12.08$. Free-stream turbulence increases the vortex shedding frequency in the post-lock-in region but does not change the system natural frequency. It also substantially increases w'_{yV} in the U_{r0} range of $1.45 < U_{r0} < 8.21$ range and w'_{yM} in the U_{r0} range of $9.18 < U_{r0} < 12.08$. These features are further studied using flow-induced forces deduced from vibration data. The overall effect of free-stream turbulence can thus be interpreted from the ratio of energy increment; free-stream turbulence feeds energy to the cylinder in general, and this energy transmission reaches a maximum at the lock-in point, and drops rapidly in the off-lock-in region. Therefore, the lock-in region is of main concern when free-stream turbulence is present.

1. Introduction

It is well known that flow-induced vibrations of bluff bodies in a cross-flow is affected by a host of excitations; chief among them are instability-induced excitation, movement-induced excitation and extraneously induced excitation (Naudascher and Rockwell, 1994). These excitations are associated with the vortex-induced force, the motion-dependent force and the turbulence-induced buffeting force, respectively. The buffeting force is present as long as there is free-stream turbulence in the oncoming flow and is not dependent on the motion of the bluff bodies (So and Savkar, 1981). This effect is derived from the flow around the bluff bodies and the behavior in the wakes. For example, in the case of a flow past a single cylinder, a strong effect of free-stream turbulence is observed in the states of transition of the wake, the shear layers, and the boundary layers (Zdravkovich, 1997). Consequently, free-stream turbulence promotes

*Corresponding author.
E-mail address: mmmcso@polyu.edu.hk (R.M.C. So).

0889-9746/$ - see front matter © 2007 Elsevier Ltd. All rights reserved.
doi:10.1016/j.jfluidstructs.2007.10.013

critical transition at a Reynolds number (Re) lower than that for a nonturbulent uniform flow. (From this point on, for the sake of brevity, the phrase "uniform flow" is used to denote "nonturbulent uniform flow") Here, Re is usually defined with respect to the mean free-stream velocity U_∞ and the hydraulic diameter of the bluff bodies. Experimental measurements of the behavior of the mean drag coefficient $\bar{C}_D$ versus Re reveal that the Re, where the drag crisis occurs, is reduced as free-stream turbulence increases (So and Savkar, 1981). Free-stream turbulence, therefore, has a major effect on the buffeting force and hence the vibration behavior of the bluff bodies.

The effect of free-stream turbulence on flow-induced forces of a single rigid cylinder in a cross flow has been investigated extensively, and several review papers (Farell, 1981; Basu, 1986; Niemann and Holscher, 1990; Ribeiro, 1992) are available. In general, free-stream turbulence alters the mean and fluctuating pressure distributions around 4the cylinder, hence, the fluctuating drag and lift forces. It also affects the frequency (or its non-dimensional counterpart Strouhal number, $\mathrm{St} = U_\infty/f_s^* D$) and the spanwise correlation of vortex shedding. Here, f_s^* is the vortex shedding frequency and D is cylinder diameter. Most of these studies only focused on the subcritical and the critical transition regimes.

In the early subcritical regime ($\mathrm{Re} = 1350$–8000), Ko and Graf (1972) showed that free-stream turbulence with low turbulence intensity (up to 4%) gives rise to a reduction in $\bar{C}_D$, but increasing the turbulence intensity beyond 4% results in an increase in $\bar{C}_D$. Surry (1972) studied the effect of free-stream turbulence in the subcritical regime ($\mathrm{Re} = 3.38 \times 10^4$–$4.42 \times 10^4$) and found that St is shifted from 0.19 to 0.22. Furthermore, the frequency peaks in the pressure spectra are lowered but broadened. This suggests that the spectral distribution of energy covers a wider frequency range. The root-mean-square (r.m.s) value of the drag coefficient C'_D is increased significantly, but the r.m.s lift C'_L is not much affected. The peak bandwidths of the lift spectra are rather broad though.

On the other hand, So and Savkar (1981) carried out a systematic study of the lift and drag force in an Re range covering the subcritical to the transitional regime ($\mathrm{Re} = 2 \times 10^4$–$3 \times 10^5$) of a single rigid cylinder in a cross flow. When Re is increased from $\sim 5 \times 10^4$ (the upper regime of transition in shear layers) to $\sim 10^5$ (the precritical regime of transition in the boundary layers), the distributions of static pressure for uniform and turbulent flows experience a change from being almost identical to being significantly different (static pressure for turbulent flow is larger), then back to being almost identical. The mean drag shows similar trend. As for the fluctuating lift and drag, it was found that their spectra vary significantly in the precritical range when Re changes from 1×10^5 to 3×10^5. At $\mathrm{Re} = 1 \times 10^5$, both lift and drag are periodic for a uniform upstream flow while fairly random for a turbulent oncoming flow. Again, this suggests that the energy fed to the cylinder covers a wider frequency range. Nevertheless, a distinct frequency peak at 0.3 can be identified from the lift spectrum; this is substantially higher than the corresponding value of 0.2 observed for a uniform flow. When Re is increased to 2×10^5, the lift remains periodic while the drag appears to be random for a uniform flow. However, the lift and drag appear to be relatively more random compared to the lower Re case. The St value at this Re shows a dramatic jump from 0.2 to 0.5. When Re increases to 3×10^5, both lift and drag appear to be random even for a uniform flow, and no distinct frequency peak can be identified. This implies that the character of the flow-induced force has been switched from that of vortex-induced to buffeting behavior. The $\bar{C}_D$, C'_D, and C'_L values show a dramatic drop at $\mathrm{Re} = 1 \times 10^5$ when free-stream turbulence is present. In fact, this is evidence of a transition region shift to lower Re.

West and Apelt (1993) measured the fluctuating pressure on a circular cylinder at almost the same Re range ($\mathrm{Re} = 10^4$–2.5×10^5), and derived the lift and drag forces. Free-stream turbulence increases the r.m.s pressure in the stagnation region. The dominant peak in the pressure spectrum is broadened and its magnitude is reduced. West and Apelt (1997) further calculated the spanwise correlation coefficients, and showed that free-stream turbulence gives rise to a substantial reduction in the correlation coefficients when free-stream turbulence promotes early transition to turbulent boundary layers. Blackburn and Melbourne (1996) measured the spanwise distribution of the lift coefficient in the range of $\mathrm{Re} = 1 \times 10^5$–$5 \times 10^5$, from which the r.m.s value, the spectrum, and the spanwise correlation of the lift were derived. It was found that C'_L is significantly reduced by free-stream turbulence in the early critical transition range. With increasing turbulence intensity, C'_L decreases to a very low value first, and then increases back. However, in the transition range, C'_L is barely affected but the bandwidth of the lift spectrum was dramatically increased by about six times. The Strouhal number was slightly increased by free-stream turbulence. This finding is consistent with that reported by So and Savkar (1981). The spanwise correlation length of the lift was also calculated. It was found that free stream turbulence reduces the correlation length. Similar to the behavior of C'_L, with increasing turbulence intensity, the correlation length drops and then increases slightly.

Compared with the investigations on rigid cylinders, studies of the effect of free-stream turbulence on flow-induced vibration of elastic cylinders are scarce. Blackburn and Melbourne (1997) carried out forced vibration tests of a cylinder in a turbulent flow at $\mathrm{Re} = 1.6 \times 10^5$. The amplitude of the cylinder displacement is $0.03D$, and the reduced velocity $U_r = U_\infty/f_e D$ is varied from 4 to 6. Here, f_e is the frequency of external excitation to the cylinder. The measured lift force was decomposed into two parts: one correlated to cylinder motion, and the other uncorrelated and termed as

residual. The spectra of the total lift are very similar to those with the cylinder stationary, except for the presence of sharp peaks at the frequencies of forced cylinder vibration. The magnitude of motion-correlated lift coefficient is much smaller than that for a nonturbulent uniform flow. Moreover, the motion-correlated lift is dominated by the acceleration-correlated lift, while the velocity-correlated lift is nearly zero.

In the present study, the effect of free-stream turbulence on flow-induced vibration of an elastic cylinder is investigated experimentally. The range of Re studied varies from 5×10^3 to 4.1×10^4, thus straddling the intermediate subcritical range. To a certain extent, this choice of Re is limited by the capability of the wind tunnel used for the present investigation. A turbulence generation grid is used to generate homogeneous, isotropic turbulence in the approach flow. The turbulence intensity as determined from the flow velocity measured using a laser Doppler anemometer (LDA) is around 10%. In the experiments, a fixed-fixed elastic cylinder model is allowed to freely vibrate in a cross-flow. The vibration displacement at cylinder mid-span in the cross-flow direction is measured using a laser vibrometer from which flow-induced force is deduced. Extensive data analysis is carried out to investigate the effect of free-stream turbulence on the dominant frequencies, the amplitude of cylinder vibration, and the flow-induced force. In addition, an energy analysis is carried out to obtain an overall understanding of the turbulence effect.

2. Experimental set-up

2.1. Wind tunnel and turbulence generation grid

Experiments were carried out in a wind tunnel at the Department of Mechanical Engineering, The Hong Kong Polytechnic University. The wind tunnel has a 2400-mm-long test-section with a 600 mm × 600 mm cross-section. The approach flow U_∞ can be continuously varied from 0 to 40 m/s. In the experiment, a turbulence generation grid was installed at the exit of the contraction section to generate homogeneous, isotropic turbulence in the test-section. A grid of the square mesh type (Fig. 1) was adopted. The dimensions of the grid are: $d_g = 20$ mm is the bar diameter and $l_g = 50$ mm is the mesh size (grid opening plus the bar diameter). When the turbulence generation grid is installed, the U_∞ range is reduced to 0–25 m/s.

Turbulence intensity of the approach flow was determined from the measured flow velocities using a LDA and can be defined as

$$\mathrm{Tu} = \frac{u'}{\bar{u}}, \tag{1}$$

where the measured instantaneous velocity in the streamwise direction is denoted as u, its time mean value as $\bar{u}$ and its r.m.s value as u'. In the experiment, u was measured across a portion of the cross-section located at $x = -60$ mm, as illustrated in Fig. 2. Turbulence intensity was calculated from the measured u using Eq. (1). The distributions of $\bar{u}$ and Tu across the indicated portion are plotted in Figs. 3 and 4, respectively, for three different Re (i.e., Re = 5000, 24 790, and 41 000), thus showing that the grid generated turbulent flow is homogeneous over the range of Re measured. The probability density functions of Tu for the three Re investigated are shown in Fig. 5. It can be determined that Tu is around 10% for the Re studied.

The power spectral density (PSD) function of u was calculated using the data measured at the center of the cross-section located at $x = -60$ mm, as shown in Fig. 6. Only the results for Re up to 24 790 are shown in the figure because the frequency range of the PSD function for higher Re is too short to be representative. The PSD functions imply that the turbulent flow velocity is a low-frequency, wide-band random process. Furthermore, the values of turbulence intensity are calculated from the PSD functions by integrating them over the frequency domain and then taking the square root of the integration. The results for Re = 5000, 14 880 and 24 790 are Tu = 13.3%, 9.83% and 10.1%, respectively. Overall, the values are around 10% except at the lowest Re. This is consistent with the results determined from Fig. 5. As a reference, the turbulence intensity for the uniform flow case is about 0.2% as reported by So et al. (2000). The present investigation examines the effect of free-stream turbulence around 10% on the flow-induced vibration and flow-induced lift force of an elastic cylinder.

2.2. Cylinder model

An acrylic tube is used as the elastic cylinder model. The outer and inner diameters of the tube are 30 and 26 mm, respectively, thus the aspect ratio is 20, and the blockage ratio is 5%. Consequently, the range of Re, in terms of the U_∞ range available and the diameter D of the cylinder, varies from 5000 to 41 000. According to Zdravkovich (2003), this Re range lies in the intermediate stage of the shear layer transition regime. The reduced velocity $U_{r0} = U_\infty / f^*_{n0} D$,

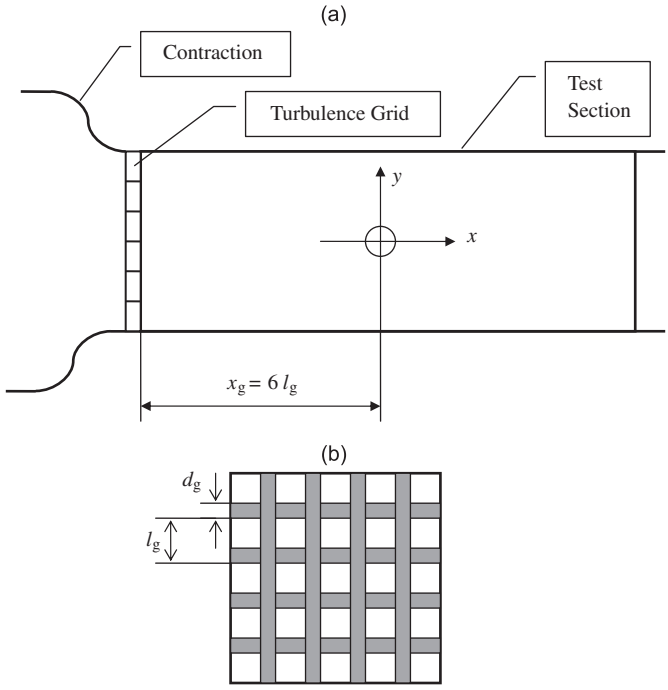

Fig. 1. Illustration of the wind tunnel with turbulence generation grid installed: (a) wind tunnel and (b) turbulence generation grid.

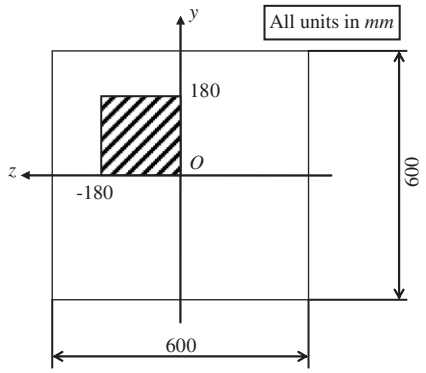

Fig. 2. Illustration of the portion of the cross-section (shadowed) located at $x = -60$ mm where turbulence intensity is evaluated from the measured flow velocity.

calculated based on f^*_{n0}, the fundamental natural frequency of the cylinder in still air, varies from 1.45 to 12.08, thus straddling the lock-in region of the vortex-induced vibration. In terms of the bar diameter ($d_g = 20$ mm) and the mesh size ($l_g = 50$ mm), this Re range becomes 3333–27 333, and 8333–68 333, respectively.

The cylinder model was horizontally mounted in the mid-plane of the test section and 300 mm downstream from the exit plane of the contraction (also the turbulence generation grid when it was installed). Both ends of the cylinder were clamped to the walls of the wind tunnel. Natural frequency and damping ratio of the cylinder model in still air were measured by the method of impulse excitation. A series of impacts were applied to the cylinder model at its mid-span. The response was measured by a vibration testing system. In the system, the vibration signal was picked up by a laser vibrometer (Polytec; Model OFV 3001) and conditioned by a charge amplifier. Afterward, the signal was sampled by the LabView system and recorded in a personal computer. The power spectrum of the response was then estimated using Welch's method implemented by the MATLAB signal processing toolbox, from which the fundamental natural frequency and damping ratio are determined to be $f^*_{n0} = 69$ Hz and $\zeta_s = 0.120$, respectively. The properties of the cylinder model are summarized in Table 1.

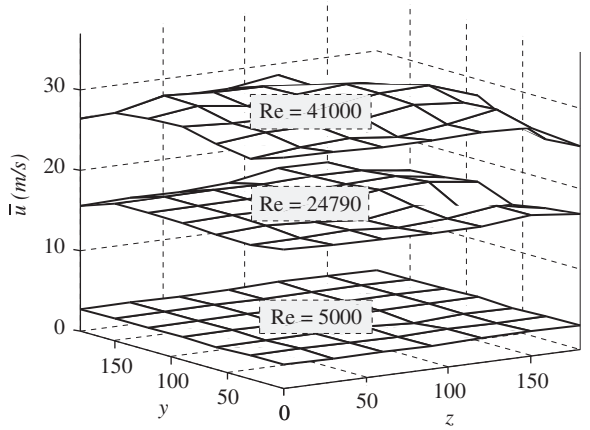

Fig. 3. Distribution of $\bar{u}$ across the portion of cross-section located at $x = -60$ mm for different Re.

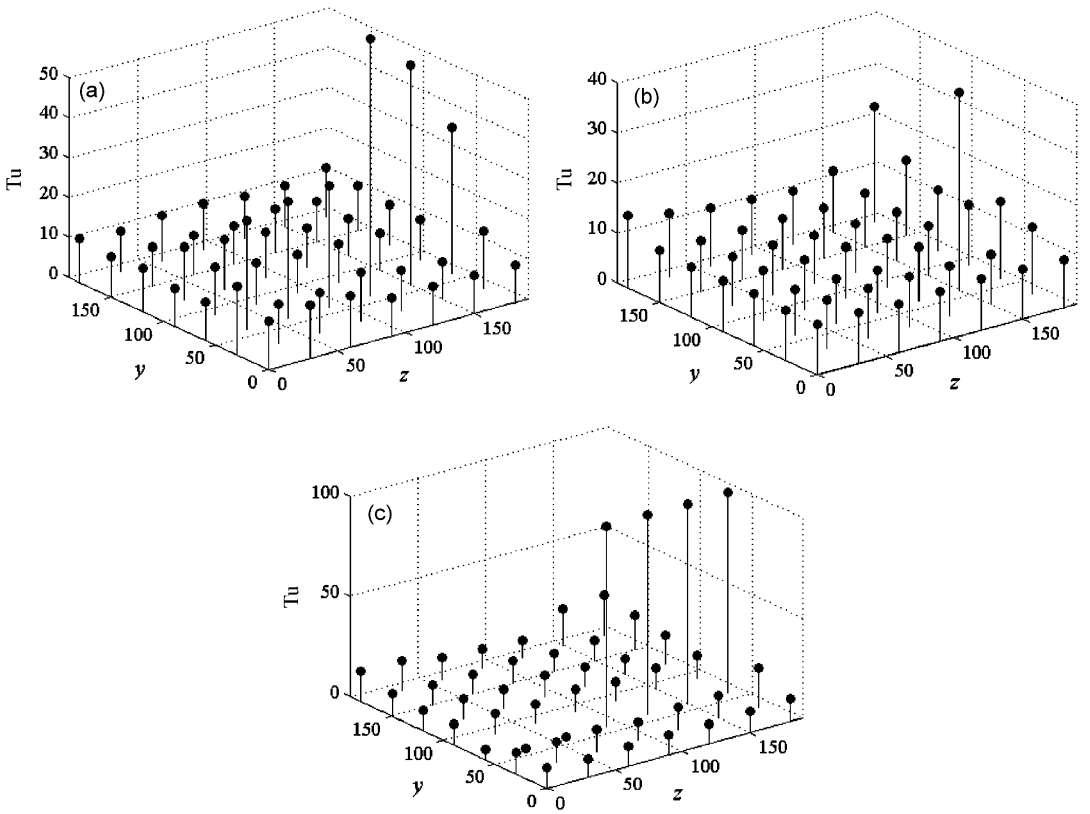

Fig. 4. Distribution of turbulence intensity across the portion of cross section located at $x = -60$ mm for three different Re: (a) Re = 5000, (b) Re = 24 790 and (c) Re = 41 000.

2.3. Measurement of cylinder vibrations

In the experiment, U_∞ is increased from 3 to 25 m/s, and cylinder displacement at the mid-span was measured, using the same laser vibrometer, for a number of mean velocities when the turbulence generation grid was absent or present. The measurements are non dimensionalized with respect to U_∞ and D for further analysis.

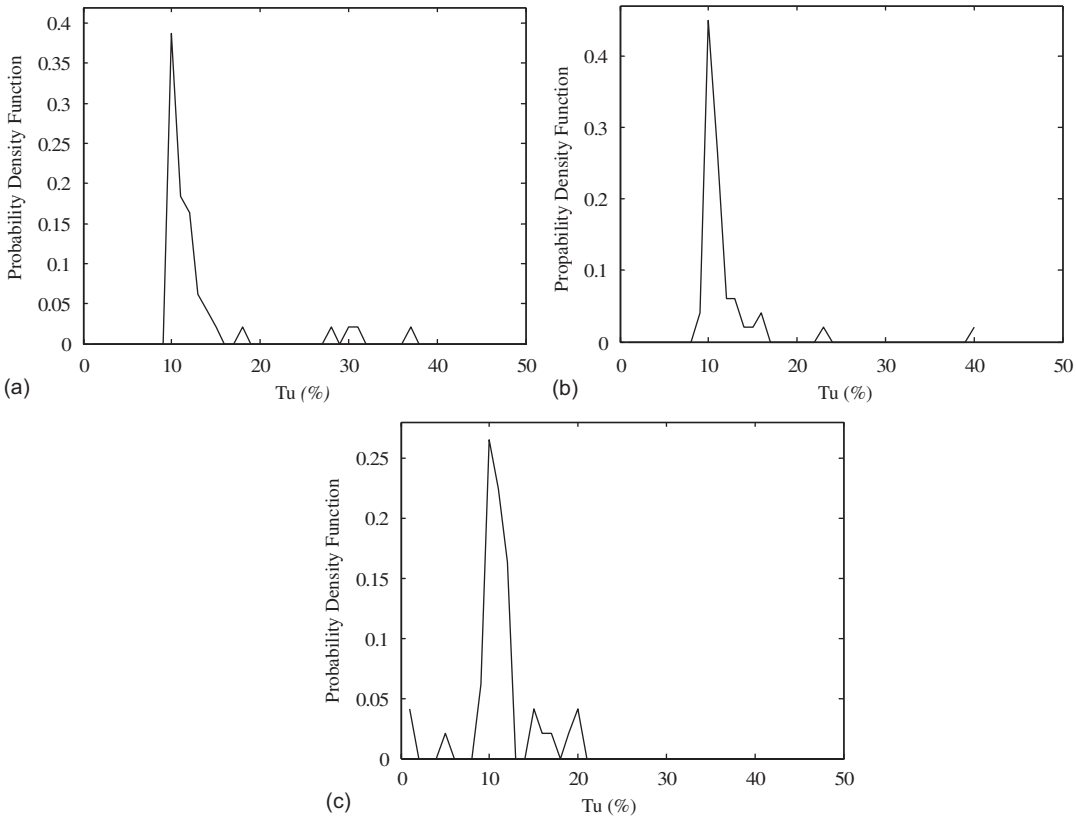

Fig. 5. Probability density functions of Tu across the portion of cross section located at $x = -60$ mm for three different Re: (a) Re = 5000, (b) Re = 24 790 and (c) Re = 41 000.

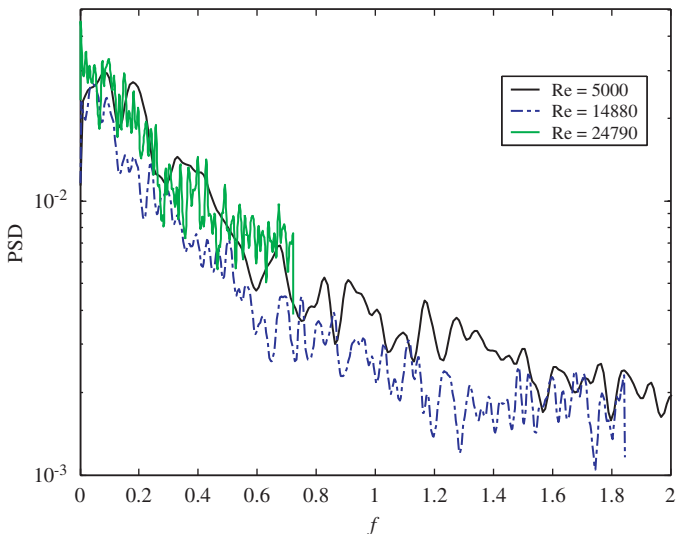

Fig. 6. Power spectral density (PSD) functions of the fluctuating flow velocity at the center of the cross-section located at $x = -60$ mm for three different Re.

Table 1
Properties of the elastic cylinder model

Cylinder material	D (mm)	M (kg/m)	EI (N m^2)	M_r	f_n^* (Hz)	ζ_s
Acrylic	30	0.208	11.8	195.5	69	0.12

Preliminary spectral analysis of the measured data showed that there exists an extremely low-frequency component (close to $f = 0$, where f is the dimensionless frequency) at some reduced velocities. This component is due to the direct-current (DC) shift of the laser vibrometer and should be eliminated in order to obtain true information about the amplitude of vibration due to fluid flow. Furthermore, there is some low-frequency components around $f = 0.05$. They could be attributed to the vibration and the end effect of wind tunnel walls (Shirakashi et al., 1985), thus should be removed also.

Consequently, a filter based on continuous wavelet transform (CWT) is applied to the measured data to filter out the low-frequency components. In the present preliminary data processing, the CWT-based filter is applied to the measured cylinder displacements with the lower frequency bound set at $f_1 = 0.0009 \approx 0$ and the higher frequency bound set at $f_2 \approx 0.05$, i.e., a high-pass filter is actually used with a cut-off frequency around 0.05.

3. Results and discussion

The primary quantity measured is the vibration displacement at mid-span of the cylinder for different free-stream flow conditions. For every case with free-stream turbulence, its counterpart with a uniform free-stream is also investigated. Altogether 12 different cases are studied. The effect of free-stream turbulence on the vibration displacement is analyzed first. This is followed by an examination of the induced-force behavior as deduced from the vibration displacement measurements. Finally, the free-stream turbulence effect on vibration energy is studied in detail.

3.1. Turbulence effects on flow-induced vibration

Using the filtered data, r.m.s values of cylinder displacements at the mid-span, w'_y, are calculated as functions of U_{r0}, for both uniform and turbulent oncoming flows. The results are shown in Fig. 7(a). It can be seen that a peak value occurs at $U_{r0} = 5.31$. This is a lock-in point at which the frequency of vortex-shedding f_s^* (or in dimensionless form St) coincides with the natural frequency of the system. For the uniform flow case, a noticable feature is that the level of cylinder vibration in the range of $U_{r0} = 8.21$–12.08 is high, almost the same as that in the lock-in point. When free-stream turbulence is present, the peak remains at $U_{r0} = 5.31$ but its magnitude is significantly increased. The level of cylinder vibration in the range of $U_{r0} = 8.21$–12.08 is also substantially increased but it is not as high as the peak value observed at the lock-in point.

The ratio of increment of displacement squared, defined as

$$r_w = \frac{w'^2_{yt} - w'^2_{yu}}{w'^2_{yu}}, \tag{2}$$

where w'_{yu} and w'_{yt} are r.m.s values of the displacement for uniform and turbulent flow, respectively, which are calculated and the results are plotted against U_{r0} in Fig. 7(b). It can be seen that the ratio has a peak value around 17 at $U_{r0} = 5.31$. However, the fluid-cylinder system is still stable as can be seen from the phase plot of w_y shown in Fig. 8. In this figure, the phase plots for two different values of U_{r0} are shown: one at the lock-in point ($U_{r0} = 5.31$) for the uniform and turbulent flow case, another at a larger value of U_{r0} for the same free-stream flow condition. It can be seen that the plots for the low U_{r0} cases display a limit cycle behavior and there is no sign of randomness. Furthermore, cylinder motions at $U_{r0} = 10.15$ for the uniform flow case and at $U_{r0} = 11.11$ for the turbulent flow case are also esentially closed loops, suggesting that the motions are still stable and are of limit cycle oscillation mode. Further discussion of the behavior of cylinder displacement is given below.

Spectral analysis of the cylinder displacement data is carried out. PSD functions of cylinder displacements are calculated using Welch's method implemented by the MATLAB signal processing toolbox, and the results are plotted as function of U_{r0} in Fig. 9. Each PSD function is normalized so that its integration along the frequency domain gives the square of the r.m.s value. It can be seen that there are two peaks in the PSD: one occurring at the vortex shedding

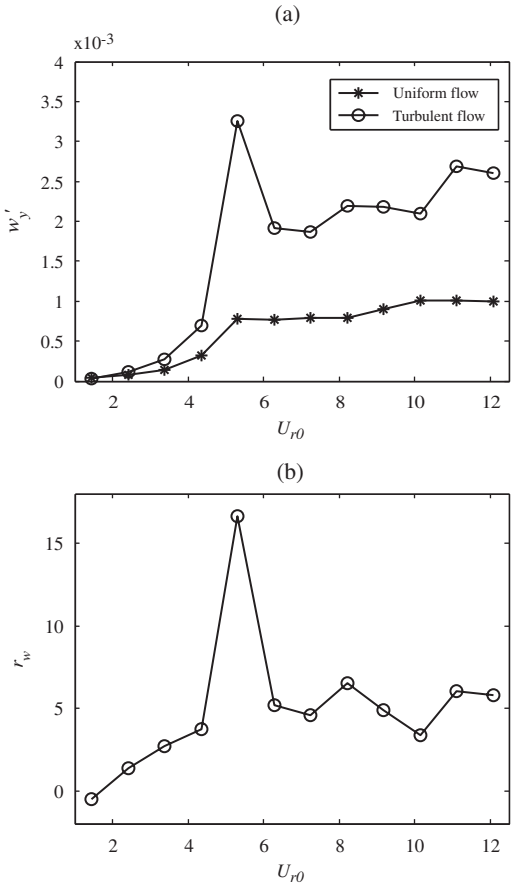

Fig. 7. Cylinder displacements at mid-span versus U_{r0}: (a) w'_y and (b) r_w.

frequency, St, another occurring at a frequency close to that of the fundamental natural frequency of the cylinder in still air f_{n0}. This implies that the displacement has two components corresponding to these two peaks, denoted as w_{yV} and w_{yM}, respectively. These two peaks coincide at the lock-in point. It should be noted that the natural frequency of the cylinder is affected by the surrounding fluid flow, hence is different from that of a cylinder in still air. In this sense, it is more appropriate to consider the second peak location as the fundamental natural frequency f_n of the fluid-cylinder system. As demonstrated by the spectral analysis result given in the following, f_n is increased compared with f_{n0} in the pre-lock-in region for the uniform flow case. However, further influence of free-stream turbulence on f_n is not significant.

The appearance of the component w_{yM} implies the existence of a negative fluid-damping force, which feeds energy to the cylinder to compensate energy dissipation due to positive structural damping. As a result, the damping of the fluid-cylinder system, which is the summation of the structural and fluid damping, is approximately zero; thus, keeping w_{yM} at a constant level. This is evident from the phase maps shown in Fig. 8, where the motion of the cylinder displays a limit-cycle mode. The fluid-damping force is usually regarded as one of the motion-dependent fluid forces. Therefore, the appearance of the component w_{yM} also suggests that the motion-dependent fluid force co-exists with the vortex-induced force in vortex-induced vibration.

From the frequency spectra, the r.m.s values of the displacement components, w'_{yV} and w'_{yM}, are calculated by integrating the spectra in the frequency ranges covering their own peaks. The results are shown in Fig. 10. It should be noted that w_{yV} and w_{yM} coincide at the lock-in point, $U_{r0} = 5.31$; they cannot be separated apart from each other, thus the data at this point is not available. Their behavior away from this point is similar to that shown for w_y in Fig. 7(a). From Figs. 7 and 10, it can be seen that the level of cylinder vibration is relatively low in the pre-lock-in region. In this region, w_{yV} is dominant for both uniform and turbulent flows, implying that cylinder vibration is mainly due to vortex

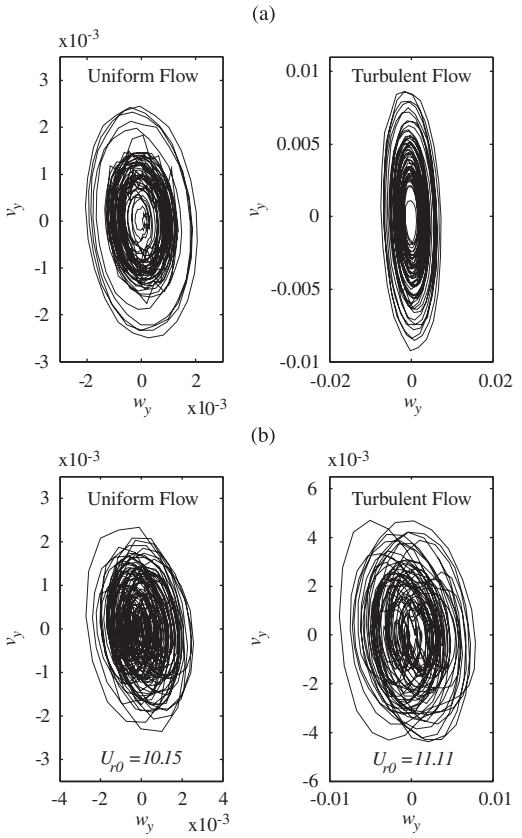

Fig. 8. Phase maps of cylinder motion: (a) lock-in region ($U_{r0} = 5.31$) and (b) region of large U_{r0}.

shedding. In the post-lock-in region, w_{yV} and w_{yM} co-exist, the latter being more and more pronounced with increasing U_{r0}, reaching a maximum value at $U_{r0} = 10.15$ for the uniform flow case and $U_{r0} = 11.11$ for the turbulent flow case (Fig. 10(a) for the plots of w'_{yV} and Fig. 10(b) for the plots of w'_{yM}). This implies that the effect of the negative fluid-damping force becomes dominant in the range of large U_{r0}.

In order to study the effect of free-stream turbulence on St and f_n, they are plotted in Fig. 11 as a function of U_{r0} for the cases of uniform and turbulent flow. Corresponding values for the cylinder in still air are also given for comparison, where St_0 is calculated using the formula given by Norberg (2003). For the uniform flow case, it can be seen that the frequency of vortex shedding, St, is increased as compared with St_0 in the post-lock-in region. As for the turbulent flow case, the frequency of vortex shedding, St, is increased in the post-lock-in region (Fig. 11(a)). This result is consistent with that reported by West and Apelt (1993). For the range $2 \leqslant U_{r0} \leqslant 12$, a linear approximation can be proposed for the variation of St with U_{r0}; it is given by $St = 0.18 + 0.005U_{r0}$. On the other hand, f_n of the fluid-cylinder system in the nonturbulent uniform flow case is increased in the pre-lock-in region, and the introduction of free-stream turbulence does not seem to have much effect on f_n (Fig. 11(b)). In fact, the effect of U_{r0} is much greater than any slight changes noticed in the variation of f_n in a uniform and a turbulent flow. Noting that w'_y is increased by about four times due to free-stream turbulence, it can be said that the main influence of free-stream turbulence is essentially on the vibration amplitude.

3.2. Turbulence effect on flow-induced force

From the above analysis of cylinder vibration data, it can be seen that the effect of free-stream turbulence on a single cylinder in a cross flow is to enhance the vibration amplitude of the cylinder. In this section, flow-induced force is deduced from the measured vibration data using the governing dynamic equation. The effect of free-stream turbulence on the flow-induced force could then be assessed.

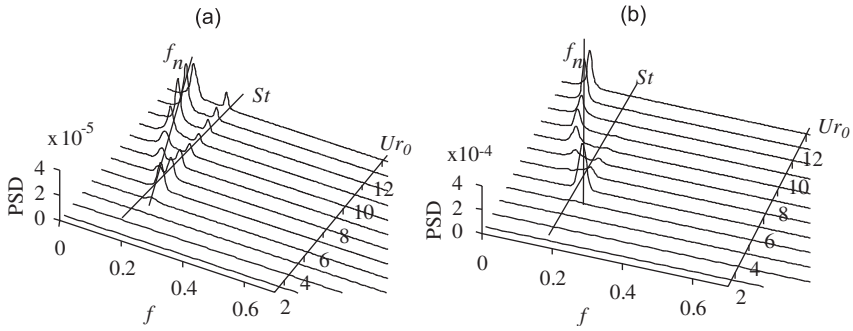

Fig. 9. Plots of power spectral density function of cylinder displacement versus U_{r0}: (a) uniform flow case and (b) turbulent flow case.

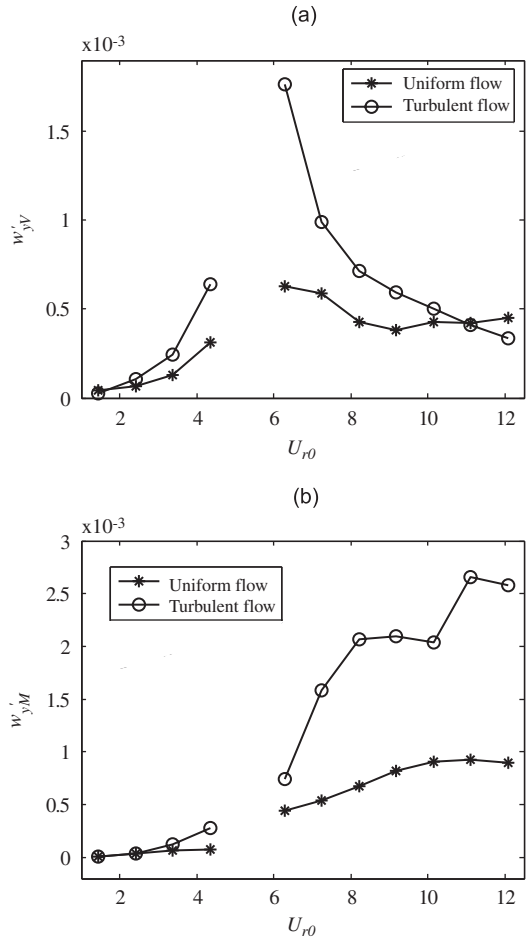

Fig. 10. Components of cylinder displacement at mid-span versus U_{r0}: (a) w'_{yV} and (b) w'_{yM}.

The cylinder used in the experiments can be modeled as an Euler–Bernoulli beam, and the equation of motion is expressed in dimensional form as

$$m\frac{\partial^2 \mathbf{w}^*(z,t)}{\partial t^2} + c\frac{\partial \mathbf{w}^*(z,t)}{\partial t} + EI\frac{\partial^4 \mathbf{w}^*(z,t)}{\partial z^4} = \mathbf{F}(z,t), \tag{3}$$

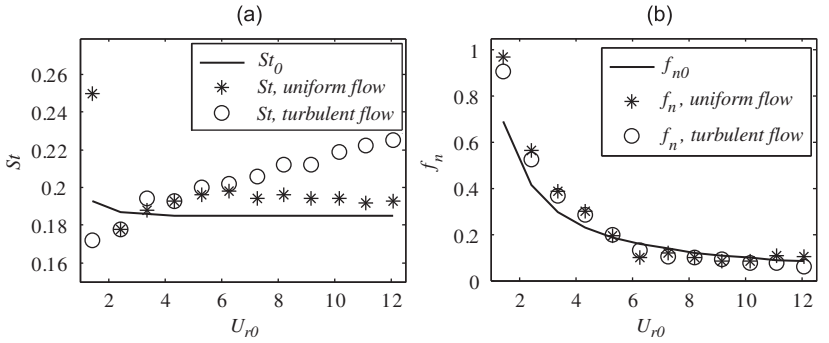

Fig. 11. Effect of free-stream turbulence on dominant frequencies of cylinder vibration: (a) frequency of vortex shedding and (b) natural frequency of the fluid-cylinder system.

where the boundary conditions are specified as

$$\mathbf{w}^*\left(-\frac{L}{2},t\right)=0,\quad \mathbf{w}^*\left(\frac{L}{2},t\right)=0,\quad \frac{\partial \mathbf{w}^*(-L/2,t)}{\partial z}=0,\quad \frac{\partial \mathbf{w}^*(L/2,t)}{\partial z}=0. \tag{4}$$

In Eqs. (3) and (4), $\mathbf{w}^*(z,t)=\{w_x^*(z,t),w_y^*(z,t)\}^{\mathrm{T}}$ is the dimensional displacement vector consisting of the displacement components in the streamwise (x) and cross-flow (y) directions, L is the length of the cylinder, EI is the bending stiffness, m and c are the mass and damping coefficient per unit length of the cylinder, respectively, and $\mathbf{F}(z,t)=\{F_x(z,t),F_y(z,t)\}^{\mathrm{T}}$ is the flow-induced force vector. Using the method of modal expansion, the solution of Eq. (3) can be expressed in the form

$$\mathbf{w}^*(z,t)=\sum_{i=1}^{N} W_i(z)\mathbf{q}_i(t), \tag{5}$$

where $W_i(z)$ is the ith normal mode shape of the undamped cylinder associated with the natural frequency f_{i0}^*, $\mathbf{q}_i$ is the generalized coordinate, and N is the number of normal modes considered. Substituting Eq. (5) into Eq. (3) and applying the orthogonal conditions, the following modal equations can be obtained,

$$\ddot{\mathbf{q}}_i(t)+2\zeta_{si}\left(2\pi f_{i0}^*\right)\dot{\mathbf{q}}_i(t)+(2\pi f_{i0}^*)^2\mathbf{q}_i(t)=\frac{\mathbf{F}_i(t)}{m},\quad i=1,2,3,\ldots,N, \tag{6}$$

where f_{i0}^* and ζ_{si} are natural frequency and structural damping ratio of the ith mode of the cylinder, respectively, and the dot represents time derivative.

In the present study, cylinder vibration is dominated by the fundamental mode; hence the modal equations can be simplified as

$$\ddot{\mathbf{w}}^*(z,t)+2\zeta_s(2\pi f_{n0}^*)\dot{\mathbf{w}}^*(z,t)+(2\pi f_{n0}^*)^2\mathbf{w}^*(z,t)=\frac{F(z,t)}{m}, \tag{7}$$

where f_{n0}^* and ζ_s are natural frequency and structural damping ratio of the fundamental mode of the cylinder in still air, respectively. From Eq. (7), the flow-induced force at the mid-span of the cylinder in the cross-flow direction can be deduced as

$$F_y(0,t)=m[\ddot{w}_y^*(0,t)+2\zeta_s(2\pi f_{n0}^*)\dot{w}_y^*(0,t)+(2\pi f_{n0}^*)^2 w_y^*(0,t)]. \tag{8}$$

Non-dimensionalizing with respect to U_∞, D, and the fluid density ρ, Eq. (8) becomes

$$c_y(0,t)=(2M_r)[\ddot{w}_y(0,t)+2\zeta_s(2\pi f_{n0})\dot{w}_y(0,t)+(2\pi f_{n0})^2 w_y(0,t)], \tag{9}$$

where c_y is the lift coefficient and M_r is the mass ratio.

The r.m.s values of the deduced force coefficient c_y' are calculated as function of U_{r0} for the uniform and turbulent flow cases and the results are shown in Fig. 12(a). It can be seen that free-stream turbulence increases the amplitude of flow-induced force. Compared to the plots for the displacement of cylinder vibration (Fig. 7(a)), it can be seen that c_y' does not reach its maximum at the lock-in point for both uniform and turbulent flows. Rather, it is relatively small at the lock-in point. The reason could be a consequence of the decrease with U_{r0} in the pre-lock-in region and its

subsequent increase in the post-lock-in region. As shown by Norberg (2003), the lift force acting on a single stationary cylinder in a cross flow undergoes a significant increment when Re varies from 3000 to 30 000. Therefore, this variation could be attributed to the effect of Re, which in the present investigation varies from 5000 to 41 000 when U_{r0} varies from 1.5 to 12.1.

Spectral analysis of the deduced force data is carried out next. PSD functions of the force data are calculated using Welch's method, and the results are shown in Fig. 13. Again, each PSD function is normalized so that its integration along the frequency domain gives the square of the r.m.s value. Similar to the cylinder vibration, the force is composed of two components, one at f_s, denoted by c_{yV}, and another at f^*_{n0} denoted by c_{yM}. Their r.m.s values, designated as c'_{yV} and c'_{yM}, are calculated from the frequency spectra and shown in Fig. 12(b) and (c). Similarly, c_{yV} and c_{yM} cannot be separated from each other at the lock-in point, $U_{r0} = 5.31$, thus the data at this point is not available.

Compared to the cylinder vibration spectra, it can be seen that c_{yV} is dominant in the whole range of reduced velocity investigated. A noticeable feature is that free-stream turbulence appears to have different effect in different ranges of U_{r0}. In order to demonstrate this further, the ratios of increment for the two force components are calculated. They are defined as

$$r_{c_{yV}} = \frac{c'_{yV_t} - c'_{yV_u}}{c'_{yV_u}} \quad \text{and} \quad r_{c_{yM}} = \frac{c'_{yM_t} - c'_{yM_u}}{c'_{yM_u}}, \tag{10}$$

for c_{yV} and c_{yM}, respectively, where the subscripts 'u' and 't' represent uniform flow and turbulent flow, respectively.

The calculated ratios are shown in Fig. 12(d) and (e). In the range of $1.45 < Ur_0 < 8.21$, the increment of c_{yV} (hence c'_{yV}) due to free-stream turbulence is significant, while that of c_{yM} (hence c'_{yM}) is large, close to the lock-in point only. The enhancement of cylinder vibration is thus mainly due to the vortex-induced force. In the range of $9.18 < U_{r0} < 12.08$, the increment of c_{yV} becomes smaller and smaller, while that of c_{yM} becomes more and more significant. Although the absolute value of c_{yM} (c'_{yM}) is smaller than that of c_{yV} (c'_{yV}), the amplitude of induced vibration is large since c_{yM} is at the natural frequency of the system. Therefore, the increment of vibration amplitude in the range of $9.18 < U_{r0} < 12.08$ is actually due to the fluid-damping force rather than the vortex-induced force.

3.3. Turbulence effect from the energy point of view

The effect of free-stream turbulence is further studied from the point of view of energy transmission. When turbulent fluctuations are generated in addition to the mean flow, energy imparted to the fluid-cylinder system is increased if the mean flow velocity remains unchanged. In general, whether the energy is transmitted to the cylinder or extracted from the cylinder, and how much this energy transmission might be, depends on the nature of cylinder vibration. This can be demonstrated by comparing the energies of the cylinder for the uniform and turbulent flow cases.

This aspect can be studied by examining the ratio of energy increment which can be defined as

$$r_E = \frac{\int_0^{f_{\max}} S_t(f)\,\mathrm{d}f - \int_0^{f_{\max}} S_u(f)\,\mathrm{d}f}{\int_0^{f_{\max}} S_u(f)\,\mathrm{d}f}, \tag{11}$$

where $S_u(f)$ and $S_t(f)$ are the PSD functions of the energy at the same U_∞ for the uniform and turbulent flow case, respectively. In the present study, the energy of the cylinder is represented by the product of the force acting on the cylinder and the cylinder velocity, i.e.,

$$P(t) = c_y(t)\dot{w}_y(t), \tag{12}$$

which is actually the power of the cylinder.

In Eq. (11), $f_{\max}$ is the upper frequency limit of integration which is determined by the sampling frequency in the experiment. For different values of U_{r0}, the dimensionless $f_{\max}$ is different. In the present study, $f_{\max}$ is taken to be 0.96, which is the minimum sampling frequency corresponding to $U_{r0} = 12.08$. The behavior of r_E as a function of U_{r0} is plotted in Fig. 14. In general, energy of the fluid is fed to the cylinder by free-stream turbulence, except for the range of small U_{r0} ($U_{r0} < 3$). A peak value occurs at $U_{r0} = 5.31$, implying that the energy imparted to the cylinder is mainly at the lock-in point. As U_{r0} decreases into the pre-lock-in region or increases into the post-lock-in region, r_E drops to a relatively low level rapidly. The behavior of r_E is similar to that of r_w as shown in Fig. 7(b). In fact, r_w indicates the increment of kinetic energy of the cylinder since the square of displacement is an indicator of kinetic energy. On the other hand, r_E represents the total energy of the cylinder, which includes the kinetic energy and the potential energy. These two energy components exchange between each other during cylinder vibration, thus the consistency between r_E and r_w is expected.

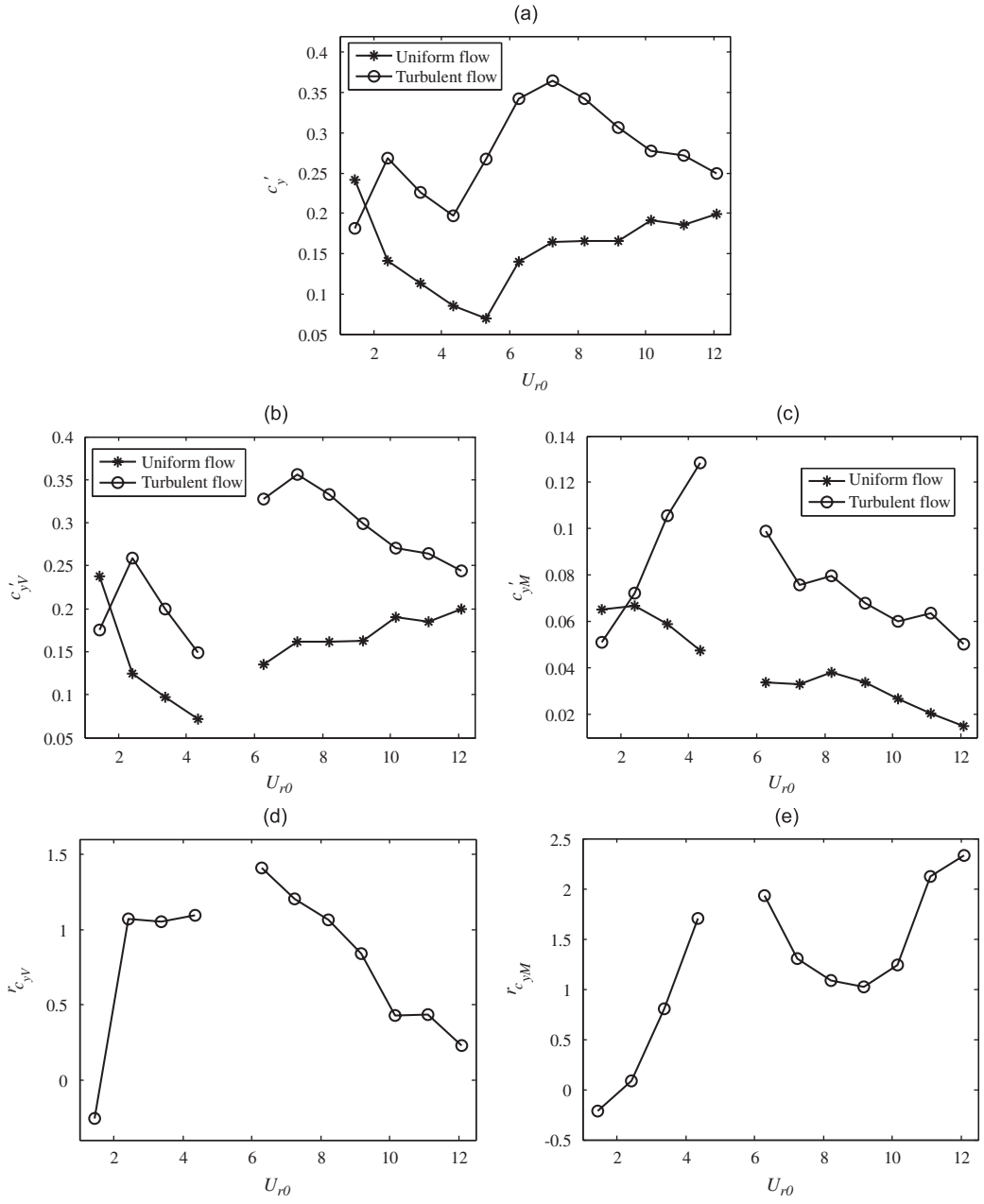

Fig. 12. Flow-induced forces at mid-span versus U_{r0}: (a) c'_y, (b) c'_{yV}, (c) c'_{yM}, (d) $r_{c_{yV}}$ and (e) $r_{c_{yM}}$.

The behavior of r_E means that the lock-in region is still the main region to be concerned when free-stream turbulence is present. The post-lock-in region is of secondary concern as can be seen from Fig. 7, where the fluid damping force is enhanced due to free-stream turbulence. It is interesting to note that the fluid-cylinder system is still stable even though energy transmitted to the cylinder is increased by a factor about 12. The evidence of stability is shown in Fig. 8, where the phase plots of the displacement show a limit cycle oscillation behavior. Although free-stream turbulence enhances the vibration amplitude and the r.m.s lift, it would not lead to instability of the fluid-cylinder system even when Re is in the range where lock-in would occur.

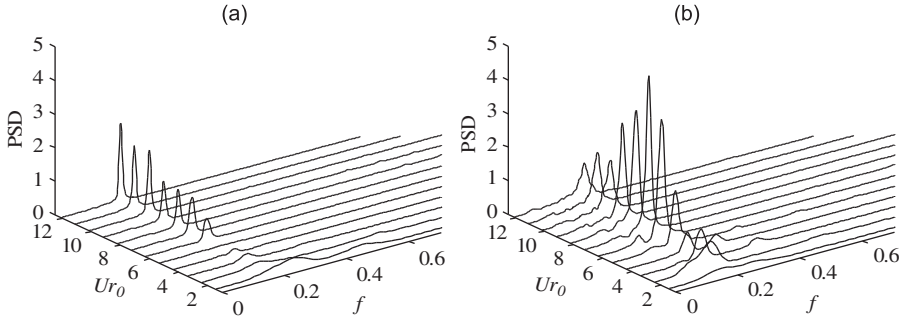

Fig. 13. Power spectral density (PSD) functions of the fluid force versus U_{r0}: (a) uniform flow case and (b) turbulent flow case.

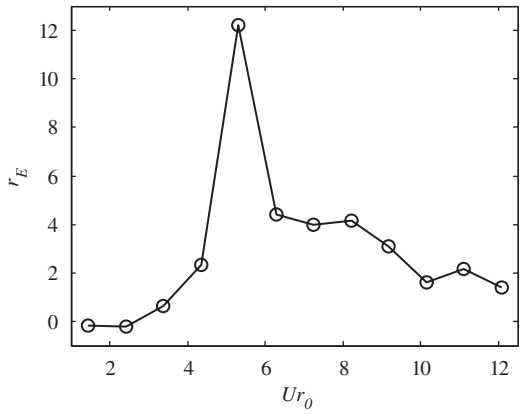

Fig. 14. Ratio of energy increment of the cylinder due to free-stream turbulence.

4. Conculsions

The effect of free-stream turbulence on vortex-induced vibration of an elastic cylinder in a cross flow was investigated experimentally. The experiments were carried out in a wind tunnel with the two ends of the elastic cylinder fixed just outside the walls of the wind tunnel. A turbulence generation grid was installed to create a homogeneous, isotropic turbulent flow with turbulence intensity around 10%.

The vibration amplitude in the transverse direction was measured at the mid-span of the cylinder. Spectral analysis of the vibration data showed that there are two dominant components: one occurring at the frequency of vortex shedding and the other at the natural frequency of the fluid-cylinder system. These displacement components are denoted by w_{yV} and w_{yM}, respectively. While w_{yV} is due to vortex-induced force, w_{yM} is considered to be maintained by the fluid-damping force. These two components coincide at the lock-in point. For the uniform flow case, w_{yV} is dominant in the range of $1.45 < U_{r0} < 7.25$. In the range of large U_{r0} values ($9.18 < U_{r0} < 12.08$), w_{yM} becomes dominant. Free-stream turbulence does not affect the range of lock-in and the natural frequency, but changes the vortex shedding frequency in the post-lock-in region, and substantially increases w'_{yV} in the range of $1.45 < U_{r0} < 7.25$ and w'_{yM} in the range of $9.18 < U_{r0} < 12.08$.

Flow-induced forces were then deduced from the vibration data. The forces thus deduced show a trend similar to the lift forces acting on a stationary cylinder, implying the component of vortex-induced force, denoted by c_{yV}, is dominant, in spite of the existence of another component at the natural frequency, denoted by c_{yM}. Free-stream turbulence appears to increase both components. The increment of c_{yV} is significant in the range of $1.45 < U_{r0} < 8.21$, whereas the increment of c_{yM} becomes more and more significant in the range of $9.18 < U_{r0} < 12.08$. This is consistent with the behavior of cylinder vibration in general.

An energy analysis showed that free-stream turbulence feeds energy to the cylinder, and the increment of the energy of the cylinder reaches its maximum at the lock-in point. The lock-in region is thus of main concern when the approach flow is turbulent.

Acknowledgments

Funding support from the Research Grants Council of the Government of the HKSAR under Projects PolyU5307/03E and PolyU5321/04E are gratefully acknowledged.

References

Basu, R.I., 1986. Aerodynamic forces on structures of circular cross-section. Part 2. The influence of turbulence and three-dimensional effects. Journal of Wind Engineering and Industrial Aerodynamics 24, 33–59.

Blackburn, H.M., Melbourne, W.H., 1996. The effect of free-stream turbulence on sectional lift forces on a circular cylinder. Journal of Fluid Mechanics 306, 267–292.

Blackburn, H.M., Melbourne, W.H., 1997. Sectional lift forces for an oscillating circular cylinder in smooth and turbulent flows. Journal of Fluid and Structures 11, 413–431.

Farell, C., 1981. Flow around fixed circular cylinders: fluctuating loads. ASCE Journal of Engineering Mechanics Division 107, 565–588.

Ko, S.C., Graf, W.H., 1972. Drag coefficient of cylinders in turbulent flow. ASCE Journal of the Hydraulics Division 98, 897–912.

Naudascher, E., Rockwell, D., 1994. Flow-Induced Vibrations: An Engineering Guide. Balkema Publishers, USA.

Niemann, H.J., Holscher, N., 1990. A review of recent experiments on the flow past circular cylinders. Journal of Wind Engineering and Industrial Aerodynamics 24, 33–59.

Norberg, C., 2003. Fluctuating lift on a circular cylinder: review and new measurements. Journal of Fluids and Structures 17, 57–96.

Ribeiro, J.L.D., 1992. Fluctuating lift and its spanwise correlation on a circular cylinder in a smooth and in a turbulent flow: a critical review. Journal of Wind Engineering and Industrial Aerodynamics 40, 179–198.

Shirakashi, M., Ishida, Y., Wakiya, S., 1985. Higher velocity resonance of circular cylinder in crossflow. ASME Journal of Fluids Engineering 107, 392–396.

So, R.M.C., Savkar, S.D., 1981. Buffeting forces on rigid circular cylinders in cross flows. Journal of Fluid Mechanics 105, 397–425.

So, R.M.C., Zhou, Y., Liu, M.H., 2000. Free vibrations of an elastic cylinder in a cross flow and their effects on the near wake. Experiments in Fluids 29, 130–144.

Surry, D., 1972. Some effects of intense turbulence on the aerodynamics of a circular cylinder at subcritical Reynolds number. Journal of Fluid Mechanics 52, 543–563.

West, G.S., Apelt, C.J., 1993. Measurements of fluctuating pressures and forces on a circular cylinder in the Reynolds number range 10^4 to 2.5×10^5. Journal of Fluids and Structures 7, 227–244.

West, G.S., Apelt, C.J., 1997. Fluctuating lift and drag forces on finite lengths of a circular cylinder in the subcritical Reynolds number range. Journal of Fluids and Structures 11, 135–158.

Zdravkovich, M.M., 1997. Flow Around Circular Cylinders, vol. 1. Oxford University Press, Oxford.

Zdravkovich, M.M., 2003. Flow Around Circular Cylinders, vol. 2. Oxford University Press, Oxford, England.